Assessing the Mixing Quality of Hetero-Aggregates: Applying Mixing Theory to TEM Image Data

Simon Buchheiser   Orkun Furat   Volker Schmidt   Hermann Nirschl   Frank Rhein*

Simon Buchheiser, Prof. Dr.-Ing. Hermann Nirschl, Dr.-Ing. Frank Rhein*
Institute of Mechanical Process Engineering and Mechanics
Karlsruhe Institute of Technology
Straße am Forum 8
76131 Karlsruhe
Germany
Email Address: frank.rhein@kit.edu

Dr. Orkun Furat, Prof. Dr. Volker Schmidt
Institute of Stochastics
Ulm University
Helmholtzstr. 18
89069 Ulm
Germany

The hetero-aggregation of carbon black and colloidal silica in a spray flame is a promising approach to improve dispersibility and stability of carbon black. The mixing quality, i.e. homogeneity of local concentrations within the hetero-aggregate, is important for both properties, yet challenging to quantify. For this purpose, multiple TEM-EDX (Transmission Electron Microscopy with Energy Dispersive X-Ray Spectroscopy) scans are conducted on two distinct process conditions, leading to hetero-aggregates two different mixing qualities. By sampling cutouts of the images at randomized locations and applying principles adapted from classical mixing theory, hetero-aggregates are characterized with respect to mixing quality, irrespective of composition and primary particle size. Furthermore, correlation coefficient functions give insight to the length scale of primary particle clusters in the hetero-aggregates. In addition, on the basis of the *intra-aggregate* mixing state and the distribution of hetero-aggregate composition, a suitable description of the *inter-aggregate* mixing state is achieved. The developed methods present a generally valid, precise characterization of the mixing quality of hetero-aggregates.

1   Introduction

Nanoparticles are widely used in industrial products because they combine material-inherent physico-chemical properties with high surface to volume ratios [1, 2, 3]. These properties are multiplied and complemented by the functional mixing with other nanoparticle species [4, 5]. Subsequently, hetero-contacts are formed at the distinct interface of the two materials, which are of fundamental importance for the desired functional properties of the mixture [6, 7]. Recently, research on hetero-aggregates has been intensified, especially due to possible applications as battery materials [8, 9, 10]. Carbon black is added therein to improve the conductivity by ensuring electrical pathways through binder polymers and active material. Therefore, high dispersion on nanoscale levels is necessary. However, during dry mixing, cluster formation and aggregate breakage of carbon black may lead to decreased conductivity [11, 12]. Hence, in order to ease the manufacturing of batteries, methods to structure the conductive carbon are investigated [13, 14, 15].
One possible approach is the hetero-aggregation of colloidal silica nanoparticles onto the aggregate structure of carbon black in spray flames as investigated in a previous publication [16]. By sintering the two distinct materials on the primary particle level, it is possible to enhance their aggregate stability. In order

to reach the desired macroscopic properties, the hetero-aggregation process and its influencing factors have to be understood on a microscopic level. However, the resulting hetero-aggregates exhibit highly fractal nanoscale structures that consist of two different amorphous materials and therefore, a reliable characterization can be challenging. Usually, multiscale characterization yields information ranging from primary particle properties to aggregate properties [17]. Other common characterization methods for hetero-aggregates are laser light diffraction [18, 19], X-ray diffraction [20] and electron microscopy [21]. The characterization of the internal mixing of hetero-aggregates is a focal point of research because functional properties like catalytic performance or lithium transport are governed by it [19, 22]. One approach is the introduction of a heterogeneous coordination number as a measure for the quality of hetero-aggregation in which the number of hetero-contacts is compared to the number of homo-contacts [23]. This concept has been developed further by including convolutional neural networks and machine learning [24, 25]. This way, metal oxide hetero-aggregates with substantial difference in electron density are characterizable. However, due to weaker intensity contrast in high-angle annular dark-field scanning transmission electron microscopy (HAADF-STEM), carbon-based materials or materials with lower coordination numbers cannot be characterized by this method. Furthermore, both primary particle species need to be distinguishable and 3D reference is necessary, limiting the general applicability of this method. Therefore, to investigate carbon black-silica hetero-aggregates, the determination of coordination numbers is not feasible. Furthermore, the heterogeneous coordination number depends on the concentration of the respective materials, making it difficult to compare process conditions with varying concentrations.

Other possible approaches to describe mixing quality include the usage of the Rényi entropy [26]. In this context, the distribution of mixing concentrations within twin-screw extruders has been evaluated [27]. Further measures for the mixing quality are two-point correlation functions which yield information on the the state of mixing at different length scales and are directly applicable to 3D and even 2D image data [28].

An alternative methodology involves the adaptation of the empirical variance of concentration to scanning electron microscopy with energy dispersive X-ray spectroscopy (SEM-EDX). The basic principle is the evaluation of the concentration in local cutouts and comparing it with the bulk concentration. The adaption to SEM is conducted by choosing image cutouts of an investigated hetero-aggregate as samples and the whole hetero-aggregate as bulk [29, 30]. However, the use of SEM-EDX analysis is constrained by the fact that it only allows for the consideration of surface composition.

To date, only the empirical variance of local concentrations has been considered, which is significantly influenced by the size of the image cutout used for quantifying the variance and the composition of the hetero-aggregate. Hence, a quantitative comparison of mixing quality is reliable primarily for hetero-aggregates of similar shape and composition with a consistent number of particles in the considered cutout, making the characterization prone to misinterpretation. For nanoscale hetero-aggregates, TEM-EDX yields a 2D projection of the material distribution within the aggregate. More detailed information would only be available by tomography which is not feasible for a statistical analysis. Therefore, the goal of this paper is the development of a method to precisely describe the mixing quality of hetero-aggregates from TEM-EDX image data, regardless of dimension, shape and material, with a focus on the nanoscale. To the best of the author's knowledge, no such adaption of mixing theory for the determination of intra-aggregate mixing on the nanoscale has been achieved yet. Furthermore, the correlation between mixing quality on the nanoscale (*intra-aggregate*) and the macroscopic scale (*inter-aggregate*) of the hetero-aggregates poses a scientific issue which is yet to be solved. It is pivotal that the resulting measure of mixing quality is able to describe differences in mixing quality for distinctly formed hetero-aggregates, allowing the comparison of multiple manufacturing processes.

2 Materials and Methods

The manufacturing process of the hetero-aggregates considered in this paper is described in Section 5. Section 2.1 deals with the workflow used for the processing of EDX scans. Finally, relevant aspects of classical mixing theory and their adaptation to transmission images are explained in Section 2.2.
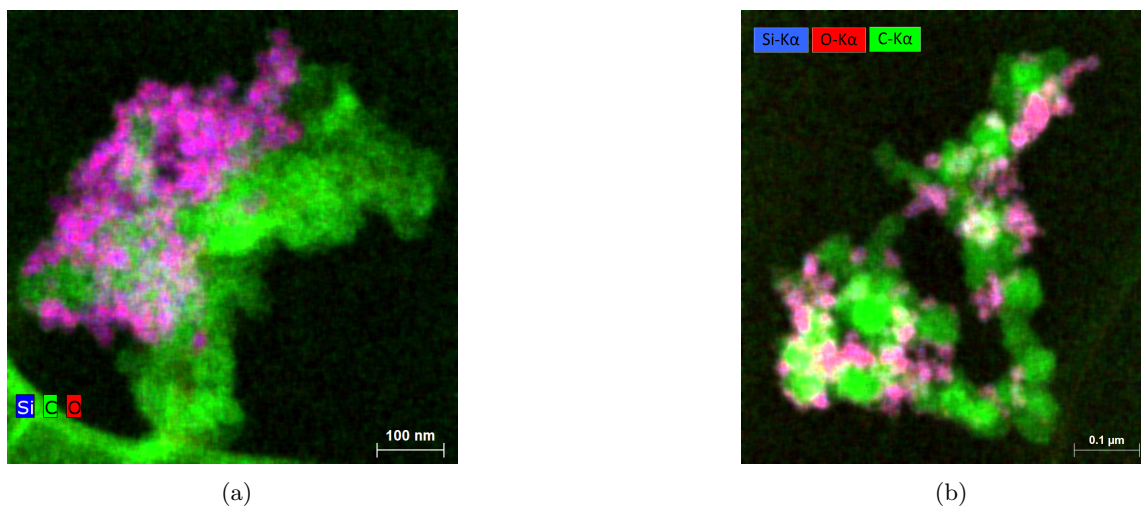
(a) (b)

Figure 1: Exemplary TEM-EDX scans of the hetero-aggregates obtained for two different process conditions. The carbon content is depicted in green, whereas the SiO_2 particles appear pinkish. (a) Hetero-aggregates with Ketjenblack-type carbon black, exhibiting segregation. (b) Hetero-aggregates with C65-type carbon black, exhibiting a homogeneous distribution of silica particles.

2.1 Image processing and sampling

For the production of the hetero-aggregates two distinct process conditions with two different kinds of carbon black were chosen. Exemplary TEM-EDX images of the synthesized hetero-aggregates are depicted in Fig. 1. For the first process conditions (Fig. 1a), denoted with KB for the Ketjenblack-type carbon black employed in synthesis, segregation was observed. On the other hand, in the hetero-aggregates synthesized with a C65-type carbon black, silica was well dispersed on top of the carbn black structure as shown in Fig. 1b. The EDX data of HAADF-STEM images provides spatially resolved detection of local silica and carbon concentrations within the hetero-aggregates. However, background noise, the lacey carbon TEM grid, and low signal strength of carbon and silicon make image processing necessary. The workflow is illustrated in Fig. 2. Separate images of the isolated signals of silicon and carbon are available directly from the EDX measurement. The images were then processed with the image editing software GNU Image Manipulation Program [31]. Concerning the carbon scan, first the lacey carbon film was edited out manually. To further reduce the background noise, a threshold was introduced. Subsequently, the images were transformed into binary images, so that the background consists of black pixels and the elemental information of white pixels. The results were two separately segmented images of the carbon and silicon distribution within the hetero-aggregate. For image analysis, a Python script has been developed in which digital cutouts with a fixed number N of particles in the cutouts are collected on $n_{samples}$ randomized locations for both carbon and silicon. Such a cutout is visualized by the rectangles in Figs. 2b and 2c. In this context, pixel-wise information on silicon and carbon content is collected. This yields the local concentration of carbon X_i in the i-th cutout, for each $i \in \{1, \ldots, n_{samples}\}$, as the number of carbon pixels divided by the total number of foreground pixels (carbon and silica) in the cutout. Encountered background pixels are ignored. Assuming a spherical projection of primary particles, the scale of the TEM-EDX scan, the mass ratio in synthesis and the mean primary particle size, the mean projected area of the primary particles is calculated. To generate an individual cutout, a random foreground pixel is selected as the center of a square whose size is chosen such that its intersection with the foreground region corresponds to the expected area of N primary particles.

2.2 Adaption of mixing theory for TEM-EDX images

In particle technology, the mixing quality is of fundamental importance for the properties of mixtures. One example is the pharmaceutical industry, where the correct amount of active ingredients in a certain product (e.g. a tablet) is crucial to ensure proper healing. It is pivotal that the homogeneity of mixtures

Figure 2: Workflow of image processing. (a) Unedited EDX scan of a hetero-aggregate. Segmented image of the carbon structure (b) and the silica structure (c) within the hetero-aggregate with evaluated image cutout. In the evaluated image cutout in (c), the silicon content is marked with dark red, the carbon content within the image cutout in mute red and the background in blue.

is high and assessed correctly, since otherwise some products will contain too much, while others contain too little active ingredients. In this context, classical mixing theory was developed in the 1950-1970s [32, 33, 34], summarized for example by J. Bridgwater [35]. Notably, P.V. Danckwerts [36] suggested the usage of two measures for the characterization of mixing quality: the intensity and scale of segregation. The basic concept of the *intensity of segregation* is the evaluation of differences between cutout and bulk concentration. In order to determine the *intra-aggregate* mixing quality, n_{samples} cutouts with a number of pixels corresponding to an area with N primary particles are evaluated at randomly chosen locations within the 2D image, see Section 2.1.

2.2.1 Empirical variance of local concentration

As already mentioned above, the local carbon concentration X_i is computed as carbon content divided by the sum of carbon and silica contents of the i-th cutout, for each $i \in \{1, \ldots, n_{\text{samples}}\}$. Furthermore, the overall carbon concentration P of a given hetero-aggregate is known directly from TEM-EDX data. By evaluating the differences between local and hetero-aggregate carbon concentrations for n_{samples} cutouts within the investigated hetero-aggregate, the empirical variance of concentration

$$s^2_{\text{intra}} = \frac{1}{n_{\text{samples}} - 1} \sum_{i=1}^{n_{\text{samples}}} (X_i - P)^2 \tag{1}$$

is obtained. Note that under some regularity assumptions on the sampling scheme, the empirical variance s^2_{intra} given in Eq. (1) converges to some limit σ^2 for $n_{\text{samples}} \to \infty$, which can be interpreted as theoretical (true) variance of local carbon concentrations. Hence, the higher the number of cutouts n_{samples}, the higher the accuracy of the empirical variance s^2_{intra}.

Analogously, the empirical variance s^2_{inter} of carbon concentration for n_{HetAgg} hetero-aggregates is given by

$$s^2_{\text{inter}} = \frac{1}{n_{\text{HetAgg}} - 1} \sum_{i=1}^{n_{\text{HetAgg}}} (P_i - \overline{P})^2, \tag{2}$$

which is a descriptor of the *inter-aggregate* mixing quality. In eq. (2) the composition of individual hetero-aggregates is compared with the mean of all hetero-aggregates. Here, P_i denotes the carbon concentration of the i-th hetero-aggregate, for each $i \in \{1, \ldots, n_{\text{HetAgg}}\}$, whereas $\overline{P}$ denotes the mean carbon concentration of the n_{HetAgg} hetero-aggregates.

2.2.2 Normalizing the variance to its bounds

Recall that the composition of the hetero-aggregates investigated in this paper consist of two different materials. However, TEM-EDX scans are considered in which either carbon or silicon content is depicted in 2D transmission images through the 3D hetero-aggregates. Hence, for pixels of the 2D images four cases are observed: Pixels that exhibit solely carbon black or silica which are denoted by [1,0] and [0,1], respectively. Because of transmission of the electron beam through the hetero-aggregate, two further cases occur, where [1,1] denotes pixels which exhibit both carbon black and silica. Finally, [0,0] denotes pixels which yield no information on the hetero-aggregates (background) and are disregarded. Depending on the composition of a hetero-aggregate, the fraction $P_{1,0}$ of [1,0] pixels associated with the hetero-aggregate and, analogously, the fractions $P_{0,1}$, $P_{1,1}$ of [0,1] and [1,1] pixels are determined, where

$$P_{1,0} + P_{0,1} + P_{1,1} = 1. \tag{3}$$

Hence, the values of $P_{1,0}$, $P_{0,1}$, and $P_{1,1}$ are (empirical) estimates of the probabilities that a pixel belongs to class [1,0] with a carbon concentration of 1, [0,1] with a carbon concentration of 0 and [1,1] with a carbon concentration of 0.5, respectively.

The notion of an *unmixed state* is common in mixing theory and represents the upper bound of the *intra-aggregate* variances s^2_{intra} given in Eq. (1) [37]. Considering an unmixed hetero-aggregate, we assume that all pixels of a local cutout only belong either to class [1,0], [0,1] or [1,1], i.e, the materials are perfectly separated. Recall that cutouts consisting of [1,1] pixels can occur even in the unmixed state due to transmission imaging. For such cutouts, the ratio of carbon and silica is equal, leading to a carbon concentration of 0.5. Thus, the variance of the unmixed state, denoted by $s^2_{\text{intra,max}}$, of a hetero-aggregate with the carbon concentration P is given by

$$s^2_{\text{intra,max}} = P_{1,0}(1-P)^2 + P_{0,1}(0-P)^2 + P_{1,1}(0.5-P)^2. \tag{4}$$

On the other hand, the empirical variance s^2_{intra} considered in Eq. (1) can take arbitrary small values and even zero, when all cutouts – by chance – exactly match the overall carbon concentration P. In practice, however, a certain lower bound $s^2_{\text{intra,min}}$ of the *intra-aggregate* variance s^2_{intra} is commonly referred to as the state of *completely random mixing* [35]. It depends on the primary particle size distributions as well as on the chosen number of particles N in the image cutout and is given by

$$s^2_{\text{intra,min}} = \frac{P(1-P)}{N} \left(\frac{d_{\text{CB,PP}}\, d_{\text{SiO2,PP}}}{d_{\text{mean,PP}}} \right)^2 \left(1 + (1-P)\,\sigma^2_{\text{SD,CB}} + P\,\sigma^2_{\text{SD,SiO2}} \right), \tag{5}$$

where $d_{\text{CB,PP}}$ and $d_{\text{SiO2,PP}}$ denote the mean primary particle diameters of carbon black and silica, respectively, and $d_{\text{mean,PP}}$ is the combined mean primary particle diameter of the two materials, depending on the carbon concentration P of the hetero-aggregate. Furthermore, $\sigma^2_{\text{SD,CB}}$ and $\sigma^2_{\text{SD,SiO2}}$ are the variances of the primary particle size distributions, by which the polydispersity of the materials is taken into account. The mixing quality index according to Ashton and Schmahl [38]

$$M_{\text{AS}} = \frac{\log(s^2_{\text{intra,max}}/s^2_{\text{intra}})}{\log(s^2_{\text{intra,max}}/s^2_{\text{intra,min}})} \tag{6}$$

ranks the empirical variance of carbon concentration of a given hetero-aggregate between 0 and 1, respective to its bounds: When the index M_{AS} equals zero, the variance s^2_{intra} of the hetero-aggregate is equal to the variance $s^2_{\text{intra,max}}$ of the unmixed state, whereas $M_{\text{AS}} = 1$ indicates that the variance of the hetero-aggregate is equal to the variance of completely random mixing [38]. Hence, the index M_{AS}, briefly called *Schmahl index* in the following, allows to characterize the mixing quality of hetero-aggregates, indifferent from carbon concentration, number of particles in the cutouts and primary particle size and, thus, represents a more objective measure for characterizing the mixing quality of hetero-aggregates.

2.2.3 Empirical covariance and correlation coefficient function

According to Danckwerts [36], the *scale of segregation* describes the state of mixing with respect to varying length scales. In this context, n_h pairs of pixels (can be considered to be cutouts with size 1 x 1) at

distances $h \geq 0$ are examined with the corresponding local carbon concentrations X_i and $Y_i = X_{j(i)}$ for each $i \in \{1, \ldots, n_h\}$, where $j(i)$ denotes the index of a pixel that has a distance of h to the pixel with index i. In other words, X_i and Y_i denote the carbon concentrations of two randomly chosen pixels, which have a distance of h from each other. For each distance $h \geq 0$ such that $n_h > 1$, the empirical covariance $C(h)$ of local carbon concentrations is then given by

$$C(h) = \frac{1}{n_h - 1} \sum_{i=1}^{n_h} (X_i - P)(Y_i - P). \tag{7}$$

Subsequently, the values $R(h)$ of the correlation coefficient function for distances $h \geq 0$, with $n_h > 1$, is given by

$$R(h) = \frac{C(h)}{s_{\text{intra,max}}^2} . \tag{8}$$

The correlation coefficient function characterizes the state of mixing at different length scales. More precisely, for values of $R(h)$ close to 1 or -1, the local carbon concentrations are strongly positively or negatively correlated at distances of h, which indicates segregation. On the other hand, values of $R(h)$ close to zero indicate that the local carbon concentrations of two pixels with a distance of h are uncorrelated, indicating a good state of mixing at that range. Therefore, if the hetero-aggregate exhibits primary particle clusters, the local concentrations are correlated more strongly over a larger distance, ultimately leading to a slower decay rate of $R(h)$.

In practice, using Eq. (8), the correlation coefficients $R(h)$ are computed for finitely many distances h from the interval $[0, h_{\max}]$ for some integer $h_{\max} > 0$, e.g., $h = 0, 1, \ldots, h_{\max}$, given that $n_0, \ldots, n_{h_{\max}} > 1$. However, the values of $R(0), R(1), \ldots, R(h_{\max})$ obtained in this way may exhibit fluctuations due to spatial variability or noise, which necessitates smoothing. This is achieved, for instance, by smoothing with a Gaussian kernel [39] to obtain a more robust and interpretable representation of the correlation coefficient function $R : [0, h_{\max}] \to [-1, 1]$ that is defined on the continuous interval $[0, h_{\max}]$. This approach enables the interpolation of the values of $R(h)$ for non-integer-valued distances h. By applying this procedure to several hetero-aggregates, n_{HetAgg} smoothed correlation coefficient functions are obtained, denoted by R_i for $i \in \{1, \ldots, n_{\text{HetAgg}}\}$. To compute the mean correlation coefficient function $\overline{R} : [0, h_{\max}] \to [-1, 1]$ for the respective set of process conditions, C65 and KB, point-wise averaging is performed, i.e.,

$$\overline{R}(h) = \frac{1}{n_{\text{HetAgg}}} \sum_{i=1}^{n_{\text{HetAgg}}} R_i(h) \tag{9}$$

for each $h \in [0, h_{\max}]$. Note that, the correlation coefficient function for the silica concentration (which results by substituting X_i by $(1 - X_i)$ and Y_i by $(1 - Y_i)$ in the computation of the correlation coefficient function) actually coincides with $\overline{R}$, due to the bilinearity of the covariances $C(h)$.

3 Results

First, in Section 3.1, the empirical variance of local carbon concentration is considered in order to determine the *intra-agregate* mixing quality of C65-type and KB-type hetero-aggregates. In this context, sampling is repeated multiple times for different numbers of primary particles in the image cutouts, to assess the dependency of the empirical variance on the number of particles within the cutouts. The initial assessment investigates six TEM-images of C65-type hetero-aggregates with perceived good mixing quality. Moreover, five TEM-images for KB-type hetero-aggregates with inhomogeneous hetero-aggregation were investigated to check if the empirical variance of local carbon concentration is able to differentiate between these mixing states. Then, in Section 3.2, 50 hetero-aggregates of the C65-type and 30 hetero-aggregates of the KB-type are evaluated at fixed image cutout sizes corresponding to $N = 25$ primary particles. In this context, the Schmahl index of each hetero-aggregate is determined for the respective variances of completely random mixing and complete segregation. Furthermore, Section 3.3 discusses how the state of *inter-aggregate*
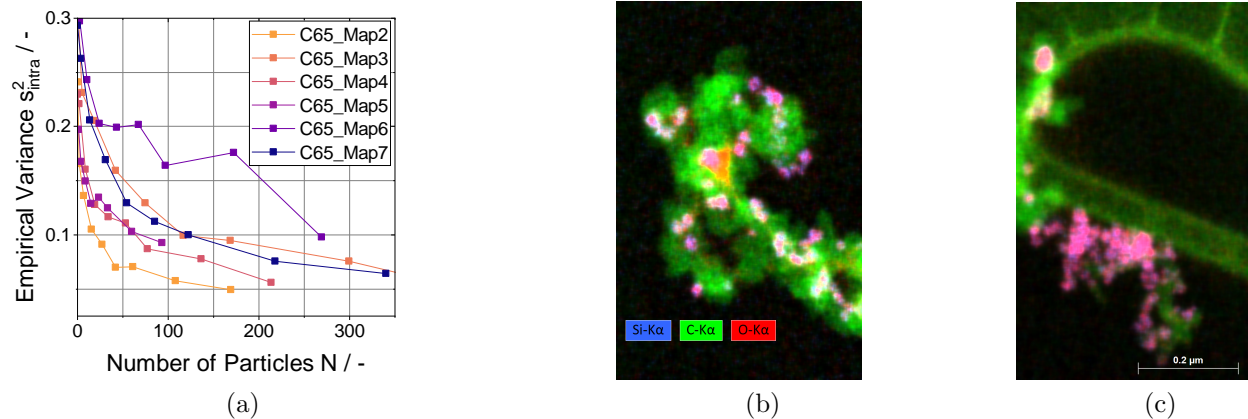
Figure 3: (a) Empirical variance s_{intra}^2 of local carbon concentration over a total of 120 cutouts for varying number of particles in the cutouts. Six segmented TEM-EDX scans of C65 type hetero-aggregates were investigated (Map2-Map7). Exemplary TEM-EDX scans of Map2 (b) and Map6 (c) with carbon (green) and SiO$_2$ (pink) signals. Map2 exhibits a homogeneous distribution of silica particles on the carbon black aggregate structure, whereas Map6 shows a cluster of silica particles, leading to a reduced mixing quality.

mixing can be described by combining the mean Schmahl index, its empirical variance and the empirical variance of hetero-aggregate concentration. Finally, Section 3.4 investigates the usage of the correlation coefficient function to characterize the *scale of segregation* in hetero-aggregates.

3.1   Empirical variance of local concentration as measure for mixing quality

In order to achieve a fundamental understanding of hetero-aggregation, a proper assessment of *intra-aggregate* mixing quality is necessary. In this context, higher deviations of the local carbon concentration in randomized cutouts result in an increased empirical variance. Consequently, a high empirical variance of carbon concentration translates into a low homogeneity of the produced hetero-aggregates. Fig. 3a depicts the changes in empirical variance of local carbon concentration of six C65-type hetero-aggregates for different numbers N of particles in image cutouts taken at 120 random locations. The figure highlights the importance of choosing a suitable number of particles within the cutouts: The smaller the number N of primary particles, the higher the resulting empirical variance s_{intra}^2. This is especially evident when a cutout of only a single pixel is taken. In this case, the variance of the unmixed state $s_{\text{intra,max}}^2$ given in Eq. (4) is obtained, as expected according to its definition. For an increasing number of particles in the cutouts, the local carbon concentration is approaching the (global) hetero-aggregate carbon concentration, resulting in a decrease towards zero. In between, the variance s_{intra}^2 is only weakly dependent on the image cutout size, resulting in a range where the values of the empirical variance of local concentration of the hetero-aggregates are sound. For a hetero-aggregate with a more homogeneous distribution of carbon and silica particles ("C65_Map2"), as depicted in Fig. 3b, the variance s_{intra}^2 is lower with a value of 0.08 for $N = 60$ primary particles in the cutouts. Remarkably, for "C65_Map6", as depicted in Fig. 3c, an accumulation of silica primary particles was present, resulting in a higher variance of 0.2 for the same number of particles in the cutouts. This shows the general feasibility of this method to quantify apparent differences in hetero-aggregate homogeneity.

Fig 4a depicts the variance s_{intra}^2 of Ketjenblack hetero-aggregates for different numbers N of particles in the cutouts, ranging from 1 pixel to 100 primary particles. It is apparent that the observed increase in variance is associated with diminished quality of hetero-aggregation. This is particularly evident in the TEM-EDX scan denoted by KB_Map3, where a nearly constant empirical variance of local concentration with $s_{\text{intra}}^2 = 0.38$ was observed, independently of the image cutout size.

However, by comparing the EDX maps in Figs. 4b and 4c, a major deficit of the empirical variance of local concentration as mixing quality criterion is highlighted: For $N = 25$ primary particles in the cutouts, both hetero-aggregates exhibit nearly the same empirical variance s_{intra}^2 of local concentration between 0.14 and 0.15, even though in Fig. 4c segregation of the materials is apparent. The similarity of variances can
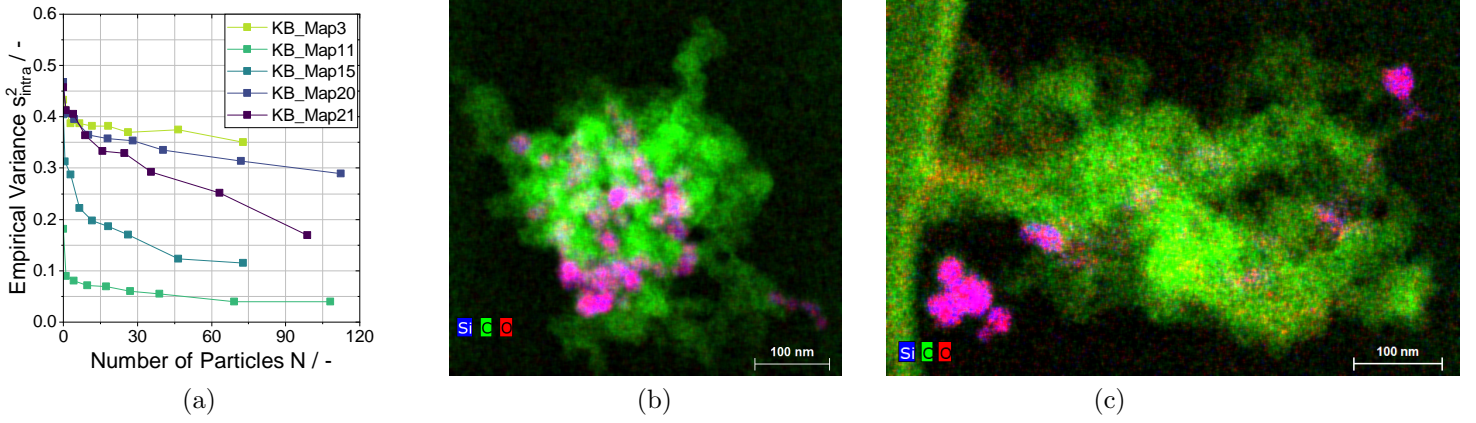
Figure 4: (a) Changes in the empirical variance s_{intra}^2 of local carbon concentration over a total of 120 cutouts for varying number of particles in the cutouts. Six segmented EDX scans of KB-type hetero-aggregates were investigated. Exemplary EDX scans of two hetero-aggregates of the KB-type (b, c) which exhibit similar empirical variances of local carbon concentration for $N = 25$ primary particles in the cutouts.

be explained by differences in concentration. The hetero-aggregate depicted in Fig. 4c exhibits a carbon content of $P = 0.92$, whereas the hetero-aggregate shown in Fig. 4b has a lower carbon content of $P = 0.77$. This means that the variance is not always suitable as a measure of mixing quality: The closer the cutout composition is towards an even distribution of the materials, the higher is the empirical variance s_{intra}^2 of local concentration. Therefore, the bounds of the empirical variance of local concentration given in Eqs. (4) and (5) have to be regarded as well in order to compare hetero-aggregates with varying compositions and primary particle sizes.

3.2 Schmahl index as metric to characterize the mixing quality of hetero-aggregates

The main advantage of mixing indices like the Schmahl index M_{AS} given in Eq. (6) is that information about composition (via the variance $s_{\text{intra,max}}^2$ of the unmixed state given in Eq. (4)) and particle size (via the variance $s_{\text{intra,min}}^2$ of completely random mixing given in Eq. (5)) is included in the mixing quality measure. Consequently, by using such measures, hetero-aggregates of different composition and particle sizes can be compared to each other in terms of their mixing quality. Fig. 5a depicts histograms of the Schmahl index M_{AS} computed from 50 EDX maps of C65-type hetero-aggregates and 30 EDX scans of KB-type hetero-aggregates, where the histogram for C65-type hetero-aggregates (purple columns) indicates that in this case the probability distribution of the Schmahl index M_{AS} can be reasonably well approximated by a conventional parametric family of distributions, such as the normal or log-normal distribution. Conversely, the probability distribution of M_{AS} for KB-type hetero-aggregates is multi-modal and, thus, does not align with conventional parametric distribution types. The mean value of mixing quality assigned by the Schmahl index M_{AS} is equal to 0.458 for the C65-type hetero-aggregates, whereas the KB-type hetero-aggregates exhibit a mean Schmahl-index of 0.557. For reference, the corresponding empirical variance of M_{AS} for all evaluated TEM-EDX maps is equal to 0.033 for the C65-type hetero-aggregates, and 0.125 for the KB-type hetero-aggregates.

In contrast to the anticipated probability distribution of the Schmahl index M_{AS} for C65-type hetero-aggregates, the distribution of M_{AS} for KB-type hetero-aggregates exhibits an accumulation of hetero-aggregates with a Schmahl index above 0.8, indicating a high *intra-aggregate* mixing quality despite the apparent segregation of carbon black and silica. Notably, the mean Schmahl index $\overline{M}_{\text{AS}}$ of 0.557 for KB-type hetero-aggregates exceeds the mean value of 0.458 for C65-type hetero-aggregates, despite the segregation of carbon black and silica qualitatively observed in TEM-EDX image data. In this context, Fig. 5b depicts an exemplary TEM-EDX image of a KB-type hetero-aggregate with $M_{\text{AS}} \approx 1$. Due to the segregation of both materials, hetero-aggregates with a skewed composition are synthesized, in which a single silica particle is sintered on top of the carbon black backbone. Sampling will naturally result in low silica concentrations, which are close to the true concentration P. Furthermore, a single primary
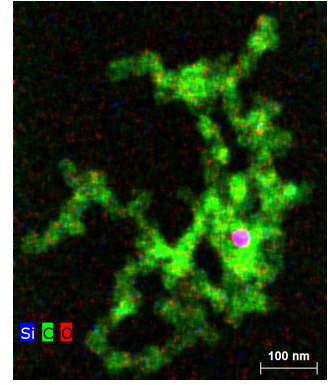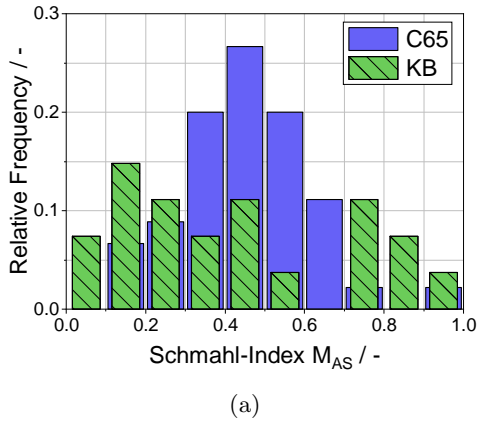
Figure 5: (a) Histograms of the Schmahl index M_{AS} for 50 TEM-EDX maps of C65-type hetero-aggregates, and for 30 TEM-EDX maps of the KB-type hetero-aggregates. The respective empirical variances of concentration were calculated on the basis of 150 cutouts and cutout sizes corresponding to $N = 25$ primary particles. (b) TEM-EDX map of a KB-type hetero-aggregate which exhibits a Schmahl index $M_{\text{AS}} \approx 1$, due to the low silica content of the hetero-aggregate.

particle can – by definition – not be clustered. Although not intuitive, this results in a Schmahl index $M_{\text{AS}} \approx 1$, independently of the position of the single silica particle. Therefore, the more segregated both materials are, the more hetero-aggregates with skewed concentrations are obtained that do not correspond to the overall mean concentration $\overline{P}$. This results in more hetero-aggregates with $M_{\text{AS}} \approx 1$. Consequently, quantifying the *intra-aggregate* mixing quality for highly segregated systems with the Schmahl index M_{AS} alone appears infeasible. This argument is supported by exclusion of all KB-type hetero-aggregates with a carbon content P above 0.95: In this test case, a mean Schmahl index $\overline{M}_{\text{AS}}$ of 0.35 with a respective empirical variance of 0.05 is obtained. In comparison to C65-type hetero-aggregates, the corrected Schmahl index of KB-type hetero-aggregates is lower while the empirical variance of the Schmahl index of KB-type hetero-aggregates is higher.

3.3 Combining Schmahl index and inter-aggregate variance

Although the *intra-aggregate* distribution of the Schmahl index M_{AS}, as discussed in Section 3.2, encompasses principal information for comparing different types of hetero-aggregates, it is insufficient to conclusively describe the *inter-aggregate* mixing state of segregated systems like KB. It is essential to also assess the distribution of concentration P to ensure a comprehensive interpretation of the mixing state. Fig. 6 depicts heatmaps of the evaluated hetero-aggregates in which the carbon concentration P of each individual hetero-aggregate is linked to its corresponding Schmahl index M_{AS}. As illustrated in Fig. 6a, the heatmap of C65-type hetero-aggregates exhibits a joint distribution of M_{AS} and P that is clustered around the respective mean values. The mean carbon concentration of 0.71 and the corresponding variance of 0.015 agree well to the mass concentration of 0.75 employed in synthesis. In contrast, the heatmap of KB-type hetero-aggregates (shown in Fig. 6b) reveals a different pattern, where aggregates are either grouped at high or low carbon concentrations. This results in a substantially higher variance in carbon concentration of the hetero-aggregates, reaching a value of 0.125, while the mean carbon concentration of these hetero-aggregates approaches the uniform mass ratio employed in synthesis, with a value of 0.61, including the hetero-aggregates with a carbon concentration > 0.95. The mean values of Schmahl index and carbon concentration are highlighted with the symbol x in Fig. 6.

In the following, we summarize these observations in a quantitative measure of mixing quality and therefore ascertain a unified description of the *inter-aggregate* mixing state. Note that the inter-aggregate empirical variance s_{inter}^2 of carbon concentration, as defined in Eq. (2), has the upper bound $\overline{P}(1 - \overline{P})$, which corresponds to the variance of a Bernoulli distribution, i.e., to the case where only hetero-aggregates with carbon concentrations of 0 and 1 occur with probability $1 - \overline{P}$ and $\overline{P}$, respectively. By linking s_{inter}^2 with the upper bound $\overline{P}(1 - \overline{P})$, the homogeneity of the carbon concentration between aggregates can be quantified
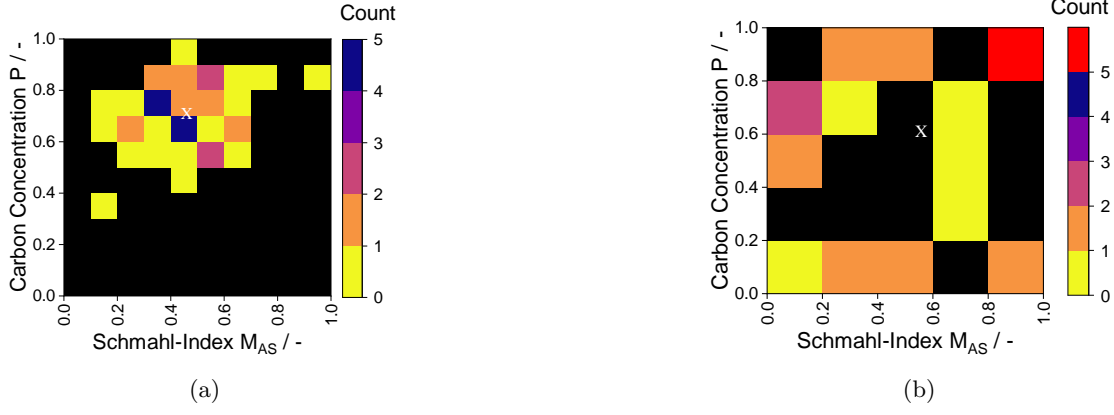
Figure 6: Heatmaps of the Schmahl index M_{AS} for two different types of hetero-aggregates and their corresponding carbon concentration P, where 50 EDX scans of C65-type hetero-aggregates (a), and 30 EDX scans of KB-type hetero-aggregates (b) have been evaluated.

by considering the mixing quality measure $\psi_P \in [0, 1]$, which is given by

$$\psi_P = 1 - \frac{s_{\text{inter}}^2}{\overline{P}(1 - \overline{P})}. \tag{10}$$

Analogously, the homogeneity of the Schmahl index between aggregates can be quantified by

$$\psi_{M_{AS}} = 1 - \frac{s_{M_{AS}}^2}{\overline{M}_{AS}(1 - \overline{M}_{AS})}, \tag{11}$$

where $\overline{M}_{AS} = \frac{1}{n_{\text{HetAgg}}} \sum_{i=1}^{n_{\text{HetAgg}}} M_{AS,i}$ denotes the sample mean of the aggregate-wise Schmahl indices $M_{AS,1}, \ldots, M_{AS,n_{\text{HetAgg}}}$, and $s_{M_{AS}}^2$ is the empirical variance given by

$$s_{M_{AS}}^2 = \frac{1}{n_{\text{HetAgg}} - 1} \sum_{i=1}^{n_{\text{HetAgg}}} (M_{AS,i} - \overline{M}_{AS})^2. \tag{12}$$

Both ψ_P and $\psi_{M_{AS}}$ are mixing quality measures that take values in the interval $[0, 1]$. More precisely, these measures quantify the variability of carbon concentrations and Schmahl indices, respectively. In particular, values of ψ_P and $\psi_{M_{AS}}$ close to zero indicate a large variance of carbon concentrations and Schmahl indices, whereas values of one indicate that each considered hetero-aggregate has the same *intra-aggregate* carbon concentration and Schmahl index. By computing the measures ψ_P and $\psi_{M_{AS}}$ for both investigated systems of hetero-aggregates, it turns out that $\psi_{M_{AS}} = 0.493$ and $\psi_P = 0.474$ for KB-type hetero-aggregates, whereas $\psi_{M_{AS}} = 0.867$ and $\psi_P = 0.927$ for C65-type hetero-aggregates. This encapsulates the distinct dispersion patterns of the 2D heatmaps of KB- and C65-type hetero-agglomerates visualized in Fig. 6.

The question remains how to define a "well-mixed" hetero-aggregate system. Based on all previous observations, we can state that a well-mixed system should possess a high average *intra-aggregate* mixing quality, while simultaneously possess narrow *inter-aggregate* distributions in mixing quality and concentration. By using the Schmahl index and the quantities derived from it as measure for the mixing quality, all these effects can be combined into a single mixing quality measure ψ_{comb}, where

$$\psi_{\text{comb}} = \frac{\alpha \overline{M}_{AS} + \beta \psi_{M_{AS}} + \gamma \psi_P}{\alpha + \beta + \gamma}, \tag{13}$$

entirely describing the mixing state of a hetero-aggregate system. In Eq. (13) the influence of the three measures $\overline{M}_{AS}, \psi_{M_{AS}}, \psi_P$ is weighted with the factors $\alpha, \beta, \gamma \in (0, 1]$ to account for specific applications. Using an equal weighting , i.e., putting $\alpha = \beta = \gamma = 1$, we obtain that $\psi_{\text{comb}} = 0.751$ for C65-type hetero-aggregates and $\psi_{\text{comb}} = 0.508$ for KB-type hetero-aggregates, finally differentiating the two process
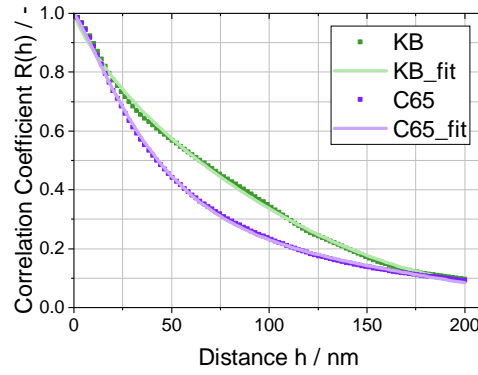
Figure 7: Correlation coefficients $\overline{R}(h)$ of carbon concentrations as a function of distance $h \geq 0$. Note that $\overline{R}$ coincides with the correlation coefficient function of SiO$_2$ concentrations, see Section 2.2.3.

conditions at a glance and encapsulating the qualitative observations in a single number. Although desirable for a quick evaluation of different processing conditions, this kind of mixing quality measure has the disadvantage of data convolution and the dilution of information. Simply speaking, a low value of ψ_{comb} could be due to any of the three involved effects, making the identification of the responsible one impossible. Thus, it is advisable to untangle the index ψ_{comb} into the three aforementioned indices to detect whether the *intra-aggregate* mixing quality is low ($\overline{M_{\text{AS}}}$), the mixing is non-reproducible ($\psi_{M_{\text{AS}}}$), or the composition of the individual hetero-aggregates is inhomogeneous (ψ_{P}) for detailed analysis.

3.4   Correlation coefficient function

Recall that, according to Danckwerts [36], the intensity of segregation and scale of segregation depict two distinct measures for the assessment of mixing quality. Hence, the behavior of the mixing quality at different length scales has been investigated by determining the correlation coefficient function $\overline{R}$: $[0, h_{\max}] \to [-1, 1]$ as given in Eq. (9). More precisely, for each the TEM-EDX image of KB-type hetero-aggregates a correlation coefficient function has been computed followed by pointwise averaging, see the green line in Fig. 7.
Analogously, the values of $\overline{R}$ have been computed for C65-type hetero-aggregates, see the purple line in Fig. 7. The significantly lower values of correlation coefficients in the range from 25 nm to 100 nm for C65-type hetero-aggregates indicate that the carbon concentrations (as well as the SiO$_2$ concentrations) at such pairs of locations have a less pronounced dependency between each other. Thus, a better mixing quality for C65-type hetero-aggregates at smaller length scales is obtained. At coarser length scales, i.e., at distances around 175 nm both hetero-aggregate types exhibit similar mixing behavior. However, the total length of most investigated hetero-aggregates spans only a few hundred nm. Hence, the correlation coefficient function at these length scales is not well defined and may not reflect the actual mixing behavior. The values of $\overline{R}(h)$ visualized in Fig. 7 can be considered as non-parametric estimates of the correlation coefficient function. Fitting a low-parametric model to these functions provides further insights, because such models are often described by interpretable parameters [40]. There are numerous parametric families of correlation coefficient functions (or covariance functions when considering the non-normalized scenario) [41]. In the case of the hetero-aggregates investigated in the present paper, it turned out that the parametric model $\overline{R}_{s_1, s_2, \nu, \lambda} : [0, h_{\max}] \to [-1, 1]$ given as a convex combination of the scaled sinc function and an exponential term, i.e.,

$$\overline{R}_{s_1, s_2, \nu, \lambda}(h) = \lambda \text{sinc}(h/s_1) + (1 - \lambda) \exp(-(h/s_2)^\nu), \tag{14}$$

for each $h \in [0, h_{\max}]$, where $s_1, s_2 > 0$ are scale parameters, $\nu \in (0, 2]$ is a parameter that controls the decay rate, and $\lambda \in [0, 1]$ controls the weighting of the scaled sinc function. Note that the parametric function given in Eq. (14) fulfills the necessary conditions for being a valid correlation coefficient function, i.e., the parametric function $\overline{R}_{s_1, s_2, \nu, \lambda}$ is positive semidefinite. By deploying `scipy.optimize.curve_fit` of the Python package Scipy [42], the parameters s_1, s_2, ν and λ have been fitted in a least squares sense,

see Table 1. Both the coefficients of determinations (R^2) of the fits (Table 1) as well as their visualizations shown in Figure 7 (dashed lines) indicate an excellent fit. It turns out that, for both KB- and C65-type hetero-aggregates, the weighing factor λ exhibits relatively low values of 0.13 and 0.22 respectively. This means that the dependence structure is dominated by the exponential term in Eq. (14). Furthermore, the parametric fit for C65-type hetero-aggregates indicates a significantly larger value of ν, i.e. $\nu = 1.19$, in comparison to KB-type hetero-aggregates where $\nu = 0.86$. Thus, with the parametric fit a quantification of the larger decay rate of the spatial correlation of SiO_2 for C65-type hetero-aggregates has been achieved. Therefore, the obtained results characterize the finer dispersion of silica particles in the C65-type hetero-aggregates and yield a description of the length scale of the hetero-aggregation. In conclusion, another key insight into the structure of hetero-aggregates that can influence their material properties is provided.

Table 1: Parameters s_1, s_2, ν, λ of the correlation coefficient function $\overline{R}_{s_1,s_2,\nu,\lambda}$ fitted to TEM-EDX image data, and coefficients of determination R^2.

hetero-aggregate type	s_1	s_2	ν	λ	R^2
KB	5.13	9.34	0.86	0.13	0.9984
C65	9.93	4.70	1.19	0.22	0.9995

4   Conclusion

In this paper, a methodology is presented to determine the mixing quality of hetero-aggregates by the analysis of TEM-EDX image data. This includes an initial assessment of the empirical *intra-aggregate* variance of local carbon concentration as well as the Schmahl index, by integrating the variances of complete segregation and completely random mixing, i.e. theoretical upper and lower bounds. Typically, the objective in the synthesis of hetero-aggregates is to maximize the number of hetero-contacts, which corresponds to a Schmahl index close to one [23]. However, for the hetero-aggregates investigated in this paper, the mean Schmahl index was roughly equal to 0.5 which indicates a mixing state where particles are neither well-mixed nor segregated. On the other hand, the evaluation of this specific value needs to be done in context of the synthesis: Silica particles are sintered onto a pre-existing carbon black backbone. These homo-contacts between the carbon black primary particles limit the number of hetero-contacts, thereby reducing the maximum achievable Schmahl index. The KB-type hetero-aggregates showed clear segregation of carbon black and silica upon qualitative assessment. However, applying the Schmahl index to these segregated hetero-aggregates yielded unexpectedly high values close to perfect mixing. Due to a highly inhomogeneous material distribution, hetero-aggregates were synthesized in which only a single silica particle was present in the carbon black aggregate structure. Since single particles can not be clustered by definition, classical mixing theory leads to values close to one, which does not correspond to a well-mixed aggregate.

To overcome this limitation from classical mixing theory, in the this paper, the *inter-aggregate* variance in concentration and in mixing quality are taken into account to achieve a quantitative measure for the degree of segregation. A well-mixed hetero-aggregate system is characterized by a high mean *intra-aggregate* mixing quality (e.g. a Schmahl index close to one) and narrow *inter-aggregate* distributions in concentration and mixing quality. Individual measures of mixing quality are introduced that characterize each of these effects and a holistic measure is presented that encapsulates all effects. This allows for a thorough description of the mixing quality of a hetero-aggregate system by means of a single value. Moreover, the comparison between disparate experiments conducted under distinct process conditions, irrespective of primary particle size and concentration, is enabled. This paves the way for scientific exchange across a range of projects. Additionally, by assessing the scale of segregation via correlation coefficient functions, the length scale of silica clusters within the hetero-aggregate is determined.

The limitations of TEM-EDX measurements also impact the applicability of the methodology. A statistical evaluation necessitates costly and time-consuming measurements. For hetero-aggregates in which the materials exhibit distinct electron densities, less expensive HAADF-STEM images are a viable option [43].

Furthermore, false positive measurements are possible when two segregated clusters are located on top of each other in transmission. Therefore, further studies are needed to clarify how intensity and scale of segregation of hetero-aggregates are influenced by the 2D projection in TEM.

In conclusion, a generally applicable methodology is presented for the characterization of mixing quality by the analysis of TEM-EDX image data. Furthermore, the gap between *intra-* and *inter-aggregate* mixing quality is bridged through the introduction of a combined mixing quality measure. By including correlation coefficient functions, both the intensity and scale of segregation are considered. Hence, the presented methodology facilitates a paradigm shift towards a more accurate and precise determination of the mixing quality of nanoscale hetero-aggregates.

5   Experimental Section

Synthesis of the hetero-aggregates:
For the production of the hetero-aggregates two distinct process conditions with two different kinds of carbon black were chosen. In both cases, the carbon black was suspended in ethanol with silica particles. The silica particles were synthesized using the Stoeber process [44]. The hetero-aggregates are then synthesized in a SpraySyn-burner by atomizing the suspension of carbon black and silica in ethanol in a spray flame. A more detailed description of the experimental setup is available in [16, 45]. Exemplary TEM-EDX images of the synthesized hetero-aggregates are depicted in Fig. 1. For the first process conditions, in which segregation was observed, the hetero-aggregates were synthesized by dispersing 30 nm silica particles with Ketjenblack (KB) (Nanografi technology, Turkey) carbon black at a weight ratio of 1:1, with a mass concentration of 0,5 weight-% of carbon black with standard SpraySyn conditions (Fig. 1a). For the second process conditions, the silica particles were finely dispersed on top of the carbon black backbone as depicted in Fig. 1b. These hetero-aggregates were synthesized by dispersing TIMCAL Super C65 (Nanografi technology, Turkey) with 10 nm silica particles at a weight ratio of 3:1. The mass concentration of carbon black was 0.5 weight-% in ethanol and the synthesis was conducted with standard SpraySyn conditions. Accordingly, the hetero-aggregates synthesized at these process conditions are referred to as KB-type and C65-type respectively.

Characterization:
Number-based size distributions of the primary particles of carbon black were obtained by statistical analysis of HAADF-STEM (FEI Tecnai Osiris, FEI company, USA) images using ImageJ. The corresponding mean particle diameter of the silica particles $d_{50,0}$ +/- one standard deviation of the number-based size distribution is averaged over a triple measurement, which was determined by dynamic light scattering (Zetasizer nano ZS, Malvern Panalytical, United Kingdom). The particle size distributions of all materials considered in this work are available in the Supporting Information.

Supporting Information
The primary particle size distributions of the used materials are available through the Wiley Online Library. All used original and segmented TEM-EDX data is available at DOI 10.35097/ptpkymb8ueq97v5d. The developed Python script is available upon publication.

References

[1] A. Camenzind, W. R. Caseri, S. E. Pratsinis, *Nano Today* **2010**, *5*, 1 48.

[2] C. A. Gray, H. Muranko, *Journal of Occupational and Environmental Medicine* **2006**, *48*, 12 1279.

[3] M. E. Spahr, D. Goers, A. Leone, S. Stallone, E. Grivei, *Journal of Power Sources* **2011**, *196*, 7 3404.

[4] A. K. Al-Kamal, M. Hammad, M. Y. Ali, S. Angel, D. Segets, C. Schulz, H. Wiggers, *Nanotechnology* **2024**, *35*, 22 225602.

[5] V. Kolck, J. Witte, E. Schmidt, H. Kruggel-Emden, *Powder Technology* **2023**, *429* 118963.

[6] M. J. Height, S. E. Pratsinis, O. Mekasuwandumrong, P. Praserthdam, *Applied Catalysis B: Environmental* **2006**, *63*, 3 305.

[7] J. Witte, Z. C. Hua, V. Kolck, H. Kruggel-Emden, S. Heinrich, E. Schmidt, *Processes* **2023**, *11*, 11 3243.

[8] W. An, J. Fu, J. Su, L. Wang, X. Peng, K. Wu, Q. Chen, Y. Bi, B. Gao, X. Zhang, *Journal of Power Sources* **2017**, *345* 227.

[9] L. Cao, J. Huang, Z. Lin, X. Yu, X. Wu, B. Zhang, Y. Zhan, F. Xie, W. Zhang, J. Chen, H. Meng, *Journal of Materials Research* **2018**, *33*, 9 1219.

[10] F. Frankenberg, M. Kissel, C. F. Burmeister, M. Lippke, J. Janek, A. Kwade, *Powder Technology* **2024**, *435* 119403.

[11] E. Asylbekov, J. Mayer, H. Nirschl, A. Kwade, *Energy Technology* **2022**, *11* 2200867.

[12] H. Bockholt, W. Haselrieder, A. Kwade, *Powder Technology* **2016**, *297* 266.

[13] Y. Yao, J. Zhang, L. Xue, T. Huang, A. Yu, *Journal of Power Sources* **2011**, *196*, 23 10240.

[14] J. Meng, Y. Cao, Y. Suo, Y. Liu, J. Zhang, X. Zheng, *Electrochimica Acta* **2015**, *176* 1001.

[15] P. Lv, H. Zhao, J. Wang, X. Liu, T. Zhang, Q. Xia, *Journal of Power Sources* **2013**, *237* 291.

[16] S. Buchheiser, F. Kistner, F. Rhein, H. Nirschl, *Nanomaterials* **2023**, *13*, 12 1893.

[17] J. Stahl, C. Mahr, B. Gerken, S. Pokhrel, A. Rosenauer, L. Mädler, *Powder Technology* **2024**, *448* 120305.

[18] J. Men, S. R. Kolan, A. Massomi, T. Hoffmann, J. Schmidt, E. Tsotsas, A. Bück, *Chemie Ingenieur Technik* **2023**, *95*, 1 107.

[19] M. Gäßler, J. Stahl, M. Schowalter, S. Pokhrel, A. Rosenauer, L. Mädler, R. Güttel, *ChemCatChem* **2022**, *14*, 16 e202200286.

[20] J. Stahl, J. Ilsemann, S. Pokhrel, M. Schowalter, C. Tessarek, A. Rosenauer, M. Eickhoff, M. Bäumer, L. Mädler, *ChemCatChem* **2021**, *13*, 12 2815.

[21] R. Strobel, *Journal of Catalysis* **2004**, *222*, 2 307.

[22] M. Iwao, H. Miyamoto, H. Nakamura, E. Hayakawa, S. Ohsaki, S. Watano, *Advanced Energy and Sustainability Research* **2024**, *5*, 8 2200206.

[23] V. Baric, H. K. Grossmann, W. Koch, L. Mädler, *Particle & Particle Systems Characterization* **2018**, *35*, 10 1800177.

[24] B. Gerken, C. Mahr, J. Stahl, T. Grieb, M. Schowalter, F. F. Krause, T. Mehrtens, L. Mädler, A. Rosenauer, *Particle & Particle Systems Characterization* **2023**, *40* 2300048.

[25] L. Fuchs, T. Kirstein, C. Mahr, O. Furat, V. Baric, A. Rosenauer, L. Maedler, V. Schmidt, *Machine Learning: Science and Technology* **2024**, *5* 025007.

[26] M. Camesasca, I. Manas-Zloczower, *Macromolecular Theory and Simulations* **2009**, *18*, 2 87.

[27] W. Wang, I. Manas-Zloczower, M. Kaufman, *International Polymer Processing* **2022**, *16*, 4 315.

[28] T. G. Williams, K. Kreckel, F. Belfiore, B. Groves, K. Sandstrom, F. Santoro, G. A. Blanc, F. Bigiel, M. Boquien, M. Chevance, E. Congiu, E. Emsellem, S. C. O. Glover, K. Grasha, R. S. Klessen, E. Koch, J. M. D. Kruijssen, A. K. Leroy, D. Liu, S. Meidt, H.-A. Pan, M. Querejeta, E. Rosolowsky, T. Saito, P. Sánchez-Blázquez, E. Schinnerer, A. Schruba, E. J. Watkins, *Monthly Notices of the Royal Astronomical Society* **2021**, *509*, 1 1303.

[29] S. R. Kolan, R. Wang, T. Hoffmann, E. Tsotsas, *Powder Technology* **2023**, *428* 118828.

[30] B. Daumann, J. A. Weber, H. Anlauf, H. Nirschl, *Chemical Engineering Journal* **2011**, *167*, 1 377.

[31] The GIMP Development Team, Gnu image manipulation program (gimp), version 3.0.2. community, free software (license gplv3), **2025**, URL `https://gimp.org/`, Version 3.0.2, Free Software.

[32] K. Stange, *Chemie Ingenieur Technik* **1954**, *26*, 6 331.

[33] K. Sommer, H. Rumpf, *Chemie Ingenieur Technik* **1974**, *46*, 6 257.

[34] G. Schmahl, *Chemie Ingenieur Technik* **1969**, *41*, 5 359.

[35] J. Bridgwater, *Particuology* **2012**, *10*, 4 397.

[36] P. V. Danckwerts, *Applied Scientific Research* **1952**, *3*, 4 279.

[37] P. Lacey, *Chemical Engineering Research and Design* **1997**, *75* S49.

[38] M. Ashton, F. Valentin, *Transactions of the Institution of Chemical Engineers* **1966**, *44*, 5 166.

[39] T. Hastie, R. Tibshirani, J. Friedman, *The Elements of Statistical Learning: Data Mining, Inference, and Prediction*, Springer, **2009**.

[40] M. Neumann, P. Gräfensteiner, C. Santos de Oliveira, J. Martins de Souza e Silva, S. Koppka, D. Enke, P. Huber, V. Schmidt, *Physical Review Materials* **2024**, *8*, 4 045605.

[41] S. N. Chiu, D. Stoyan, W. S. Kendall, J. Mecke, *Stochastic Geometry and its Applications*, J. Wiley & Sons, **2013**.

[42] P. Virtanen, R. Gommers, T. E. Oliphant, M. Haberland, T. Reddy, D. Cournapeau, E. Burovski, P. Peterson, W. Weckesser, J. Bright, S. J. van der Walt, M. Brett, J. Wilson, K. J. Millman, N. Mayorov, A. R. J. Nelson, E. Jones, R. Kern, E. Larson, C. J. Carey, İ. Polat, Y. Feng, E. W. Moore, J. VanderPlas, D. Laxalde, J. Perktold, R. Cimrman, I. Henriksen, E. A. Quintero, C. R. Harris, A. M. Archibald, A. H. Ribeiro, F. Pedregosa, P. van Mulbregt, SciPy 1.0 Contributors, *Nature Methods* **2020**, *17* 261.

[43] C. Mahr, J. Stahl, B. Gerken, V. Baric, M. Frei, F. F. Krause, T. Grieb, M. Schowalter, T. Mehrtens, E. Kruis, L. Mädler, A. Rosenauer, *Nano Select* **2024-04**, *5*, 4 2300128.

[44] W. Stöber, A. Fink, E. Bohn, *Journal of Colloid and Interface Science* **1968**, *26*, 1 62.

[45] F. Schneider, S. Suleiman, J. Menser, E. Borukhovich, I. Wlokas, A. Kempf, H. Wiggers, C. Schulz, *The Review of Scientific Instruments* **2019**, *90*, 8 085108.